Chapter 2

Sodium/Halide Flame Synthesis of W and W-Ti Nanoparticles

Jose Ignacio Huertas

Additional information is available at the end of the chapter

http://dx.doi.org/10.5772/62023

This chapter describes the experimental work employed to demonstrate the applicability of the particle encapsulation method to the production of high-purity unagglomerated nanosize tungsten (W), and tungsten titanium alloys (W-Ti) particles by flame synthesis. These materials possess unique properties that make them desirable for advanced applications. Some work has been carried out to produce ultrafine powders of W by flame synthesis. However, due to the high particle number densities and steep temperature gradients associated with flames, the produced W particles form long-chain agglomerates. Furthermore, pure W metal can be highly pyrophoric and an oxide contaminant is formed when the powder is exposed to atmosphere. Consequently, size, purity, and agglomeration are simultaneously the critical issues that need to be addressed in the synthesis of nanosized W.

This chapter begins by describing the existing needs for W and W-Ti nanoparticles. Subsequent sections describe the thermodynamics and experimental considerations for the synthesis of the powder. The chapter concludes by describing the experimental results obtained.

1. Need for nanosized W and W-Ti particles

Tungsten metal (W) and tungsten heavy alloys (WHA) possess unique properties that make them desirable for advanced applications. W has a very high density (19.3 g/cm3) and the highest melting point of all the elements (3410°C).

WHA are two-phase metal–matrix composites. Conventional1y they are processed by premixing the W metal with binder elements such as Fe, Ni, Cu, or Co. The mixture is then compacted in either a mechanical, hydraulic, or isostatic press and conso1idated by 1iquid phase sintering (LPS) in a protective atmosphere (hydrogen or vacuum) at a temperature where the minor constituents form a liquid. W content normally varies from 90 to 98 wt%. The final sintered microstructure consists of a contiguous network of near1y pure BCC W grains embedded in a ductile FCC matrix. The typical mean tungsten grain size varies from 30 to 60 μm. [27] WHA

have a combination of high strength (800–1000 MPa), high ductility (10–30%), good e1ectrical and thermal conductivity, corrosion resistance, and excellent machinability. [28]

Current applications for W and WHA inc1ude counterbalances in military aircraft, radiation shields, lighting components, ignition electrode materials, catalysts in the chemical industry, alloying elements for high speed steels, sputter targets in VLSI chip technology, and a variety of sport related parts. [29]

WHA are also being investigated as a replacement for dep1eted uranium (DU) alloys for kinetic energy penetrators (KEP) app1ications. Despite the excellent performance of DU alloys, replacements are being sought because of serious economical and po1itical concerns associated with the significant health risk and decontamination cost associated with the manufacture and handling of DU. W and WHA are being pursued as alternatives [30, 28] because their densities are similar to DU alloys, and high density is the primary requirement for KEP. To date, the performance of WHA under high strain rate conditions has been inferior to DU, [27] and there is a great interest in developing WHA with improved KEP performance.

Much of the work both within the Army and in the commercial sector has been based on the premise that it is only necessary to improve the quasi-static mechanical properties of WHA in order to improve bal1istic properties. Many meta1lurgical parameters have been investigated with regard to alloying elements, characteristics of the W starting powder, impurities, process parameter variations in the liquid phase sintering (LPS) cyc1e, post-sintering heat treatment, and matrix composition variations at constant W content. Although these studies have led to improvements in static properties, those improvements have not translated to improved high strain rate performance, [31] and the high strain rate properties are of critical importance for KEP applications.

DU penetration into semi-infinite targets has been shown to be characterized by localized (adiabatic) shear deformation that permits the penetrator to discard deformed material quickly along its flanks as penetration proceeds. This process leads to a “self-sharpening” effect that keeps the interface stress on the armor higher for a longer period of time. Such deformation contrasts with observations for WHA penetrators that deform by “mushrooming” at the nose, thereby spreading the impact force and lowering the interface stress and penetration distance. Figure 1 represents the deformation behavior of (a) a tungsten penetrator and (b) α Uranium alloy penetrator.

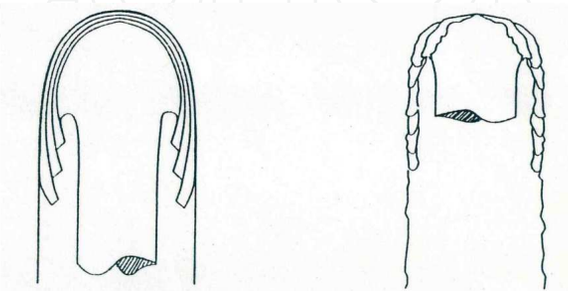

Figure 1. Representation of the deformation behavior of (a) a tungsten penetrator and (b) α Uranium alloy penetrator. [27]

It is believed that during high strain rate penetration, the WHA grains are heated under near adiabatic conditions, eventually passing through the ductile-to-brittle transition, and exhibiting flow softening at higher temperatures. [27] However, fracture events occur at the microstructural level at relatively small strains and before there has been significant heating. Cracks initiate at the W-W grain boundaries with as little as 3–5% plastic strain, and the matrix does not carry the load until ~30% plastic strain. Thus, there is a critical need to obtain control of the high strain rate penetrator performance of WHA by tailoring the initial composition and structure.

Penetration performance for WHA should be enhanced by improving room temperature plasticity at high strain rates. WHA with ultrafine grain sizes (<0.1 μm) may meet this requirement. Furthermore, low-temperature (<1500°C) densification can be enhanced during consolidation of ultrafine powders and ductility can be improved via the mechanism of grain boundary sliding. [32]

On the other hand, Magness et al. [27] have suggested replacing the ductile matrix in the WHA composite with one made of an alloy system that is more shear-prone, with a substantially lower softening temperature, to alleviate problems associated with high strain rate deformation in WHA. Metals that tend to display adiabatic shear tendencies are characterized by a low work-hardening rate, high thermal softening, and low strain rate sensitivity. In this regard, alloy systems such as titanium alloys have been recommended for matrix replacement. [27, 33]

Given the above motivation, a need exists for a W-Ti alloy with W content of 90–98 wt% and a microstructure consisting of ultrafine W grains embedded in a soft Ti matrix. The methodology proposed is to produce nanosized W, Ti, and W-Ti powders and then consolidate them at low temperature (~1000°C) to preserve grain size. Previous attempts to reach that objective have been unsuccessful because there has not been a reliable method availab1e to produce the ultrafine starting powders. [33]

Mechanical milling, [34] liquid phase synthesis, [35], [36] chemical vapor deposition (CVD), [37], [38] and gas-to particle conversion methods [22, 39, 40, 41] are possible sources of ultrafine W powders. Among these processes, flame synthesis has by far the highest possible production rates.

Production of ultrafine powders of W by flame synthesis started with Lamprey et al. [22] in 1962. In this work, an inverted coflow burner was employed to obtain submicron metal powder by hydrogen reduction of WCl_6. Future studies involved reacting tungsten halides in H_2/F_2 [40] or H_2/Cl_2 [41] flames. These approaches successfully produce W metal. Nonetheless, due to the high particle number densities and steep temperature gradients associated with flames, these processes offer poor control of particle size and morphology. Long-chain hard agglomerates were usually formed [22] (Figure l-6) and the pure metal W powders were often pyrophoric, or oxide contamination formed on exposure to atmosphere. [41]

2. Particle encapsulation to control agglomeration and oxygen impurities

The above problems are potentially avoided by using the particle encapsulation method developed by Axelbaum et al. [26], [42] and described in Section 4. Since W is produced through the reaction:

$$WCl_{6(g)} + 6Na_{(g)} \rightarrow W_{(s)} + 6NaCl_{(g)} \quad DH = -1241.3\ kJ\ /\ mole \tag{1}$$

the NaCl by-product was employed as the encapsulating material in these studies. NaCl is an effective encapsulating material because its boiling point is 1410°C, which allows condensation to be triggered in the flame by controlling temperature and NaCl concentration. The NaCl encapsulation can be removed by washing with an appropriate solvent or through vacuum sublimation at moderate temperatures (~800°C). Experimentally, the particle encapsulation process has been shown to be realizable; Ti, [42] TiB_2, [42] and AlN [43] particles encapsulated with NaCl have been obtained through the respective reactions:

$$TiCl_{4(g)} + 4Na_{(g)} \rightarrow Ti_{(s)} + 4NaCl_{(g)} \qquad DH = -393.5\ kJ\ /\ mole \tag{2}$$

$$TiCl_{4(g)} + 2BCl_{3(g)} + 10Na_{(g)}\ \ TiB_{2(s)} + 10NaCl_{(g)} \tag{3}$$

$$AlCl_{3(g)} + NH_{3(g)} + 3Na_{(g)} \rightarrow AlN_{(s)} + 3NaCl_{(g)} + 1.5H_{2(g)} \tag{4}$$

Employing similar sodium-halide chemistry (Equation 1), the NaCl encapsulation process is well suited for the production of nanosized W and W-Ti because the salt by-product is produced in the reaction zone simultaneously with the core product particles. Sodium reduction of chlorides was first employed in the 1960s in the effort to produce high-purity silicon for semiconductors and solar cells through the reaction:

$$SiCl_{4(g)} + 4Na_{(g)} \rightarrow Si_{(s)} + 4NaCl_{(g)}{}^{44} \tag{5}$$

The main difficulty with this process is separating the silicon from the reaction by-product NaCl to yield solid silicon. Gould and Dickson [44] patented an impaction technique where the reaction products form a supersonic jet exiting from the reaction chamber. The jet impinges on a flat surface, whereupon the silicon particles deposit. Calcote and Felder [45] advanced this work, producing high-purity silicon, and proposed that many other materials, including Ti and W, could be produced by sodium/halide combustion synthesis. Glassman et al. [46] also proposed extending this chemistry to other materials, developed a thermodynamic criterion for selecting appropriate reactants, and employed Na/K-halide chemistry to produce TiN, TiB_2, TiC, $TiSi_2$, SiC, and B_4C. These authors, however, did not attempt to produce W or W-Ti, or unagglomerated nanosized particles.

http://dx.doi.org/10.5772/62023

Metals	Intermetallics	Ceramics
Si*		B_4C*
Mo		TiN*
W	$MoSi_2$	SiC*
Fe	TiAl	TiC*
Al	$TiSi_2$*	HfB_2
Ta	Ti_3Al	TaB_2
Zr	Ti_5Si_3	TaC
Nb		ZrB_2
Be		WC

*Materials produced via Na/K-halide combustion synthesis.

Table 1. Materials that can be produced by sodium-halide combustion synthesis. [45, 46]

3. Thermodynamic considerations

The relevant chemistry for synthesizing W and Ti is given in Equations 1 and 2. Chlorides of tungsten titanium react with sodium vapor to produce the parent metals and the by-product NaCl. Since the reaction of metal halides with sodium is known to be extremely fast, reaction considerations are dominated by thermodynamics.46 The NASA equilibrium code and commercial software were used to guide selection of operating conditions to obtain high yields of W and W-Ti. Thermodynamic yield is defined as the ratio of the moles of metal in the products per mole of metal chloride in the reactants.

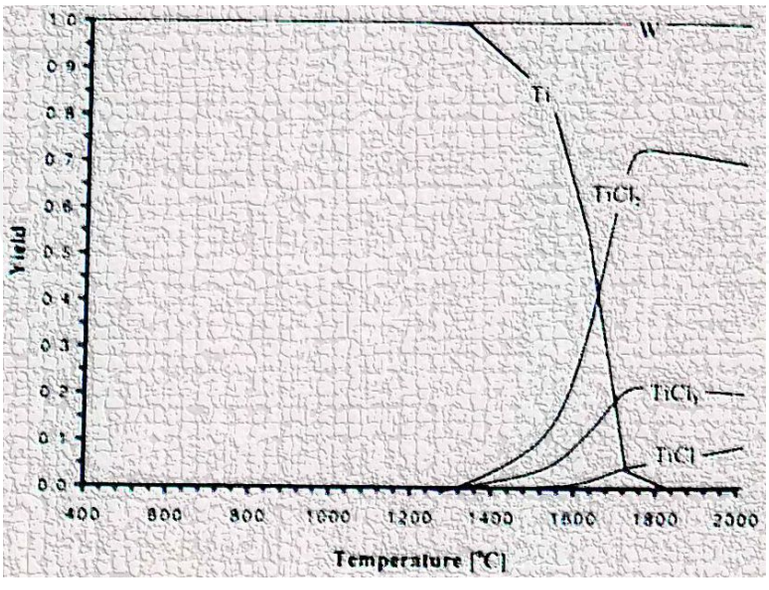

Figure 2. Equilibrium yields for the Ti/W/Cl/Na system.

Figure 2 shows the yield as a function of temperature for the W/Ti/Na/Cl system. The yield of Ti begins to drop rapidly at temperatures above ~1250 °C, yet the yield of W is 100% up to 2200°C. Various quantities of argon can be used in this process with little effect on thermodynamic yield. In a commercial system, argon can be readily recycled because at room temperature, the products are in condensed phases.

In comparison, thermodynamic calcu1ations for the W/H/C1 system, as employed in Reference 41, show that 100% yields can be obtained for tungsten, but only for temperatures below 1200°C. The reaction:

$$WCl_{6(g)} + 3H_{2(g)} \rightarrow W_{(s)} + 6HCl_{(g)} \qquad \Delta H = -60.l\ kJ / mole \tag{6}$$

is ~20 times less exothermic than Equation 1, and is thus less favorable. Furthermore, this system is not suitable for flame synthesis of Ti because the reaction:

$$TiCl_{4(g)} + 2H_2 \rightarrow Ti_{(s)} + 4HCl_{(g)} \qquad \Delta H = 393.9\ kJ / mole \tag{7}$$

is highly endothermic. The sodium/halide flame process can also be used to obtain W-Ti alloy or composite particles. The material can be produced *in situ* in a single, continuous operation. There are two ways to obtain the material: 1) by producing both metals at the reaction front:

$$TiCl_{4(g)} + xWCl_{6(g)} + \left(4 + 6x\right)Na_{(g)} \rightarrow xW - Ti_{(s)} + (4 + 6x)NaCl_{(g)} \tag{8}$$

or 2) by injecting the $TiCl_4$ downstream of the WCl_6, thus generating a new second reaction zone and producing Ti that will mix with and/or encapsulate the W. The first method is simpler but less flexible in terms of reinforcement size. In this study only the first method is considered.

4. The coflow sodium–halide burner

The coflow open atmosphere burner described in Axelbaum et al. [42, 43] is used in this study. The approach involves injection of the appropriate metal halide vapors into a laminar coflowing stream of sodium vapor. The burner consists of a set of heated concentric tubes with inner/outer diameters of 4/5, 11/13, 20/26, and 120/125 mm. Chlorides are supplied through the innermost tube, followed by Ar, then Na/Ar vapor, and finally Ar in the outermost tube. A detailed description of the burner can be found in References 42 and 43.

Tungsten chloride powder is heated in a quartz reservoir to 265°C (T_m = 275°C) yielding a saturation pressure of O.11 atm. Argon carrier gas is metered by a mass flow controller and is passed through the powder, and it is assumed that saturated conditions exist at the exit of the

http://dx.doi.org/10.5772/62023

reservoir. Liquid $TiCl_4$ heated in a stainless steel reservoir to 140°C (T_b = 136.4°C) and the flow rate of the vapor is metered with a high-temperature mass flow controller.

Sodium is heated to 150°C (Tm= 97.8°C) in a stainless steel reservoir. From there, it is pumped into the Na-vaporizer with a calibrated syringe pump. The Na-vaporizer consists of a porous cylinder wherein Ar carries Na vapor from the wetted walls. The temperature of the Na-vaporizer is fixed at 750°C where the saturation pressure of Na is 0.25 atm. Since liquid sodium at temperatures above 150°C will spontaneously ignite in air, the positive displacement syringe pump is employed to minimize the risk of uncontrolled release of liquid Sodium.

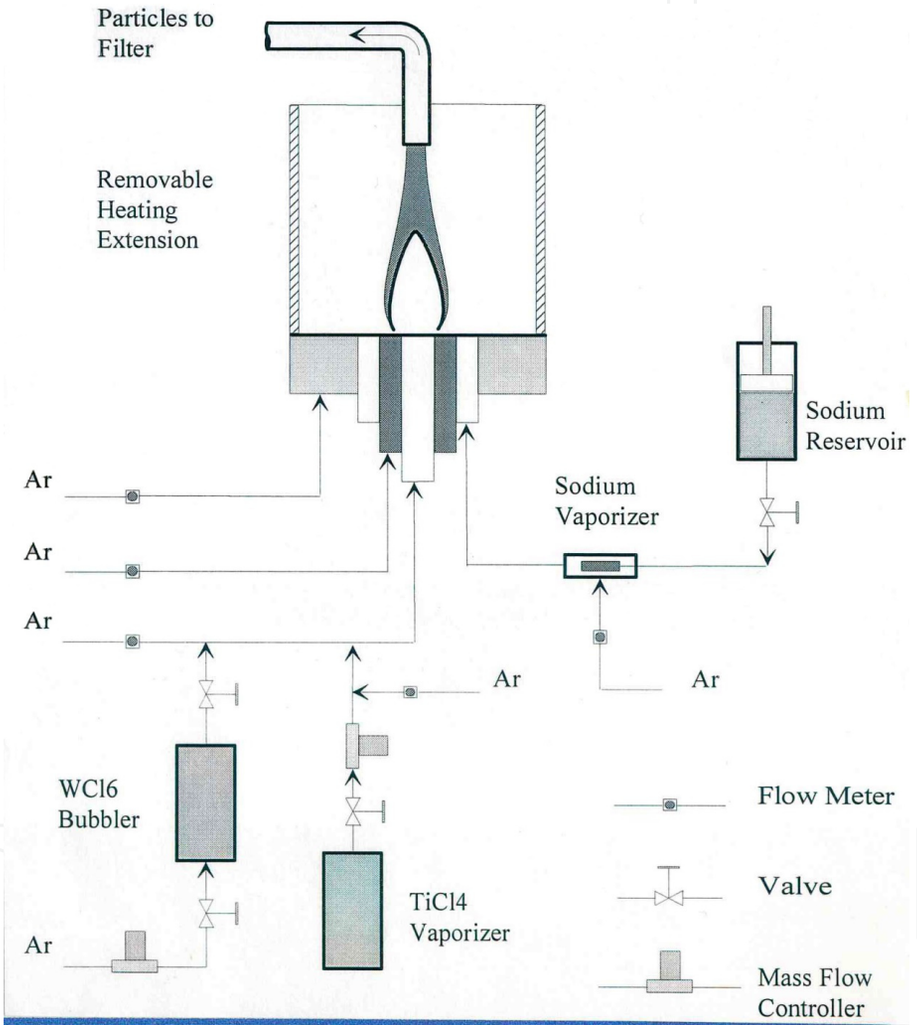

Figure 3. Burner schematic for production of W and W-Ti nanoparticles.

At the exit of the concentric tubes, reactants mix by diffusion and react spontaneously, producing a stable reaction zone. The reaction zone or flame appears as a bright yellow/orange zone having a shape similar to laminar hydrocarbon diffusion flames. Figure 4 shows a typical sodium/halide flame. Particles formed in the reaction zone are convected downstream, extracted by isokinetic sampling, and then collected onto a porous stainless steel filter.

Quantitative *in situ* laser measurements of particle size and number density have not been performed because the absorption spectrum of the sodium dimer in the visible spectrum is strong and broad. [47] Instead, an argon-ion laser is used to visually monitor scattering from particles to identify the particle-laden zones.

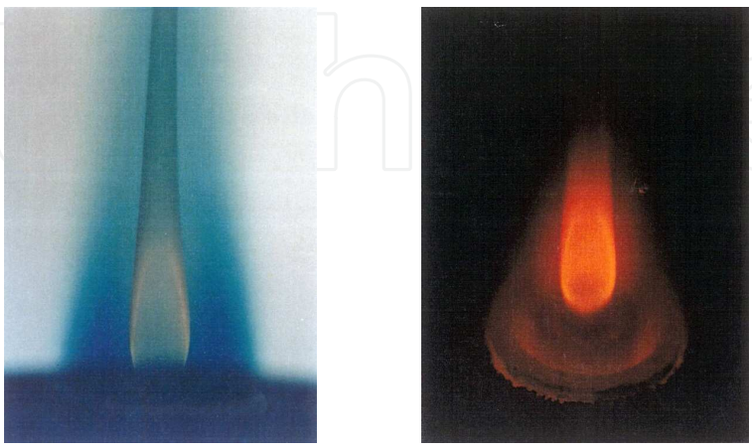

(a) (b)

Figure 4. Sodium flame for producing TiB2 nanoparticles: (a) backlit photograph (the purple/blue haze is due to light absorption by sodium vapor); (b) direct photograph from above. [42]

5. Synthesis of nanosized particles

Several runs were made to optimize the characteristics of the produced powder. The collected powders were characterized by X-ray diffraction (XRD), scanning electron microscopy (SEM), atransmission electron microscopy (TEM). XRD was used for phase identification of bulk powder samples and to obtain information about the size of the nanocrystallites using the X-ray line broadening method (i.e., the Scherrer formula). SEM and TEM studies of the powders were carried out to determine particle size distribution. Elemental composition was determined by energy disperse X-ray analysis (EDAX). Powders were exposed to atmosphere, and XRD characterization studies were performed in open atmosphere.

5.1. Production of nanosized W powders

Table 2 summarizes the various run conditions under which W powders were produced. XRD spectra of the as-produced powders show NaCl, α-W, and 5 extraneous peaks. After water washing, the salt is removed but the extraneous peaks remain (Figure 5). The extraneous peaks index reasonably well to either W_3O, W_3C, or β-W. However, β-W is a meta-stable phase that is known to stabilize to α-W [35, 36, 38] under heat treatment at temperatures greater than 450°C. Thus, the as-produced powder was heat treated under dynamic vacuum (-8×10^{-7} torr) at 800°C for 5 h. The extraneous peaks were no longer present, indicating that they were due to β-W. The remaining α-W peaks correspond to a particle size of 30 nm as determined by the Scherrer formula.

http://dx.doi.org/10.5772/62023

			Chlorine		Inner Shroud	Na		Outer Shroud
Run Number	T Burner °C	Flow SCCM	WCl_6 %	$TiCl_4$ %	Ar Flow SCCM	Flow SCCM	Na %	Ar Flow SLM
1	688	103	12		556	893	9	18.4
2	770	105	14		412	963	8	18.4
3	780	109	13		556	944	8	18.4
4	785	90	13		412	1405	15	18.4
5	640	145	4	1.0	1275	839	12	24.2
6	790	130	10	1.9	915	944	8	14.5
7	780	85	14	2.8	915	970	11	18.4
8	780	70	12	12.3	915	1229	13	18.4

Table 2. Run conditions for production of nanosized W (runs 1–4) and W-Ti (runs 5–8) powders.

For powders that were heat treated after exposure to atmosphere, XRD spectra show small peaks due to Na_2WO_4. Formation of Na_2WO_4 is due to the presence of Na in the as-produced sample. The Na is present because the flame is overventilated in Na, and thus, Na exists at the sampling location above the flame. The Na reacts with H_2O upon exposure to atmosphere, producing NaOH. During heat treatment, NaOH can react with W to produce Na_2WO_4 or $(Na_2WO_4)2H_2O$. Formation of these impurities is not an inherent concern since they can be eliminated by proper sampling and/or low temperature (~400°C) sublimation of the Na under dynamic vacuum. Indeed, XRD spectra for samples that were heat treated before being exposed to atmosphere do not show the Na_2WO_4 phase.

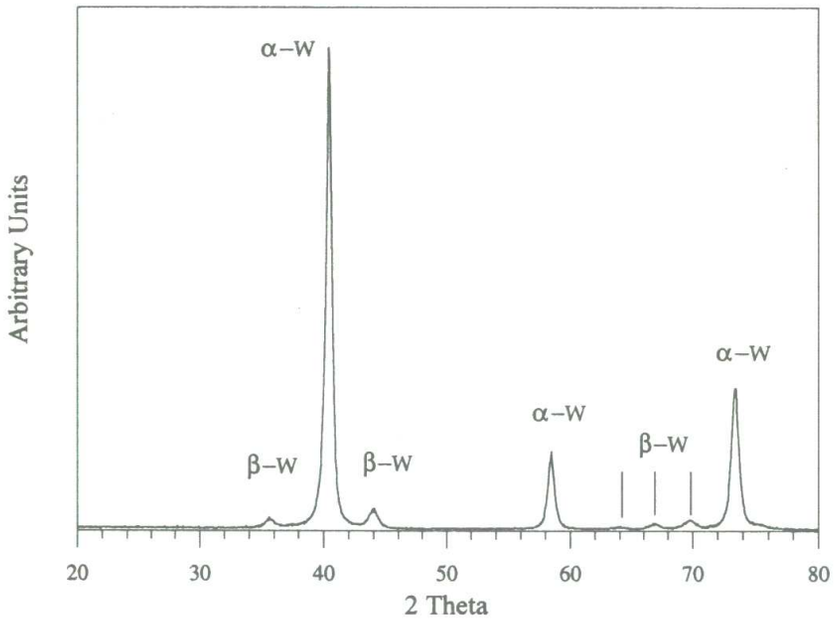

Figure 5. XRD of water-washed W sample for run No. 3.

Several batches of as-produced powder were water-washed with deionized, degassed water and dried under dynamic vacuum. A vigorous reaction was occasionally observed when the waterwashed powders were exposed to atmosphere. The sporadic pyrophoric nature of this ultrafine W is consistent with the findings for other flame-synthesized W. [22] On the other hand, the salt-encapsulated particles never reacted when exposed to atmosphere.

5.2. Production of nanosized W-Ti composites

The same configuration was used to produce nanosized W-Ti powders. Table 2 shows the run conditions. In all but run number 8, the flow rates of $WC1_6$ and $TiCl_4$ were set to obtain a ratio of 10 wt% Ti. Figure 6 shows the XRD spectra of the as-produced powders and reveals the presence of NaCl and α-W. No other phases are observed. The crystallite size of α-W determined by the Scherrer formula is ~30 nm. The XRD spectrum also does not show the presence of Ti. The Ti phase may be amorphous in the as-produced condition, or the amount of Ti may be insufficient to detect against the broad W background, or Ti may be in solid solution with W. When the powders are heat treated under dynamic vacuum (-lxl0^{-6} torr) at 850°C for 2 h, the salt is sublimed away and the XRD spectra of the heat treated samples show only broad peaks indexing to W (Figure 7). The particle size estimated by the Scherrer formula is ~40 nm, indicating that this heat-treatment does not increase the size of the W-Ti powders significantly. The sample is stable under atmospheric conditions and again there is no evidence of contamination or oxidation of the powders. The NaCl has also been removed by washing the powders with deionized, degassed water. The XRD results are similar to those obtained when the powder is heat treated.

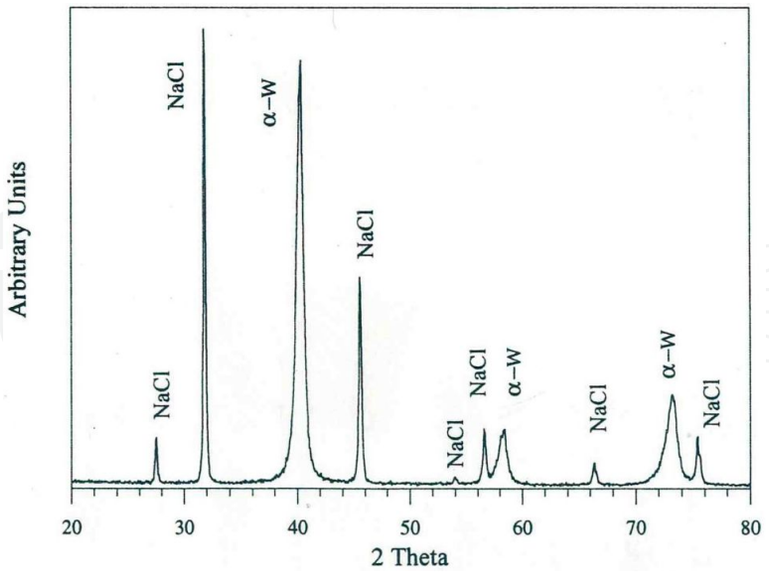

Figure 6. XRD of as-produced nanosized W-Ti for run No. 7.

SEM and TEM micrographs of the annealed W-Ti powders show particles of 40–50 nm in size. Figure 8 is a typical SEM micrograph, revealing that some of the particles are cubic while others

http://dx.doi.org/10.5772/62023

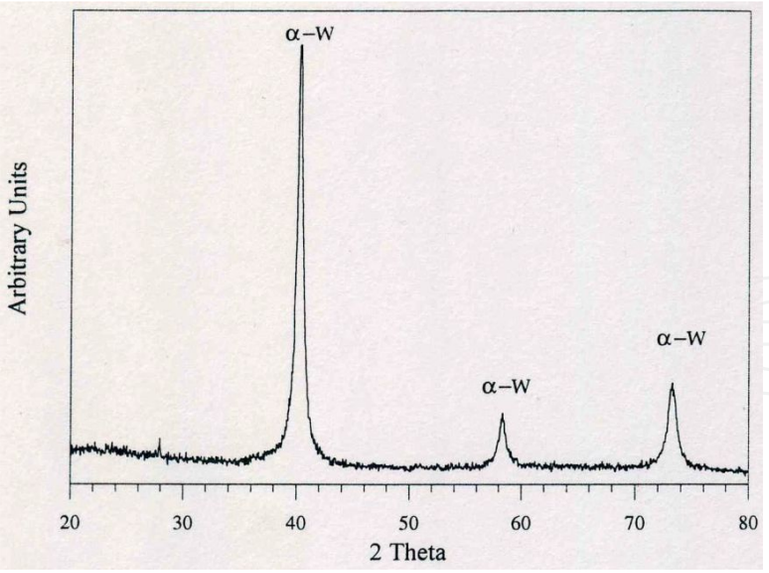

Figure 7. XRD of W-Ti sample for run No. 7, heat treated at 850°C for 8 h under dynamic vacuum.

are hexagonal. The micrograph also shows that particles are not in the form of long-chain agglomerates, but rather appear to be only loosely agglomerated. Figure 9 is a typical TEM micrograph of the as-produced particles, showing nanosized particles encapsulated in a NaCl matrix. Figure 8 together with Figure 9 show the effectiveness of the encapsulation process to control the presence of long-chain agglomerates.

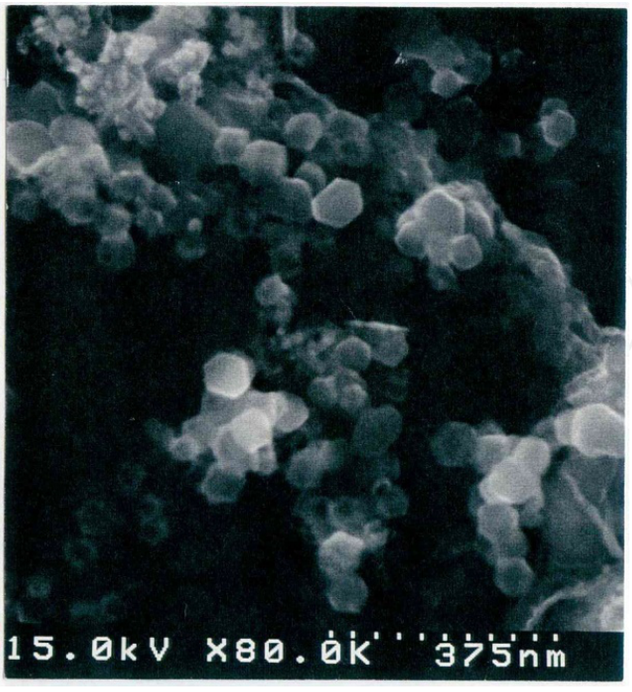

Figure 8. SEM micrograph of W-Ti sample for run No. 7, heat treated at 850°C for 2 h.

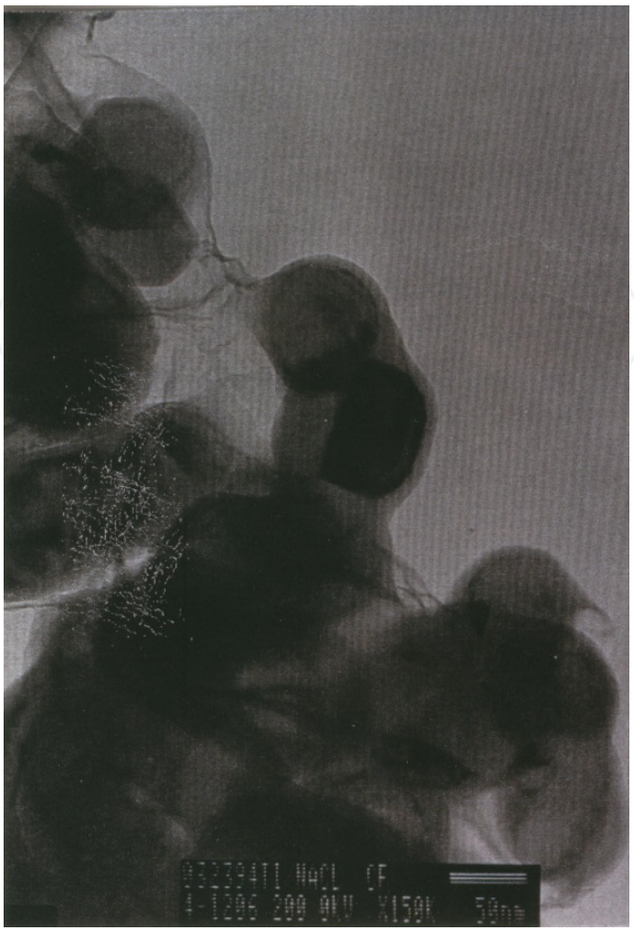

Figure 9. TEM micrograph of flame synthesized Ti particles of size ~75 nm encapsulated in NaCl.

Elemental analysis by ICP-atomic emission spectroscopy shows the presence of 15 wt% Ti. The fact that Ti is present, but not detected by XRD even after annealing, suggests that the Ti is in solid solution with W. Nonetheless, the equilibrium phase diagram of W-Ti [48] (Figure 10) shows that for this composition, Ti is also present as a separate phase, in addition to being in solid solution with W. To verify the presence of Ti as a separate phase, the effect of Ti addition on the lattice parameter was determined using XRD spectra. The experimental value of lattice parameter obtained using the XRD spectrum of the W-15 wt% Ti sample is 3.1680 x $10^{-[10]}$ m. The theoretical estimation of the lattice parameter of 15 wt% Ti in solution with W, calculated using literature values of lattice parameters for W(3.1653 x $10^{-[10]}$ m) and Ti (3.306 x $10^{-[10]}$ m), [49] and considering a linear variation of lattice parameter with alloying addition of Ti, gives 3.2500 x $10^{-[10]}$ m. This suggests that a substantial portion of the Ti is present as a separate phase.

To investigate the effectiveness of different methods of removing the NaCl from the as-produced samples, heat treated and water-wash samples were analyzed for Na and Cl (NSL Analytical Services, Inc.). Na was determined by ICP mass spectroscopy and Cl by ion chromatography. Table 3 shows the results. These tests indicate that the salt encapsulation of the particles may be effectively removed. Similar elemental analysis tests have shown the effectiveness of the NaCl encapsulation method protecting the powder from contamination

http://dx.doi.org/10.5772/62023

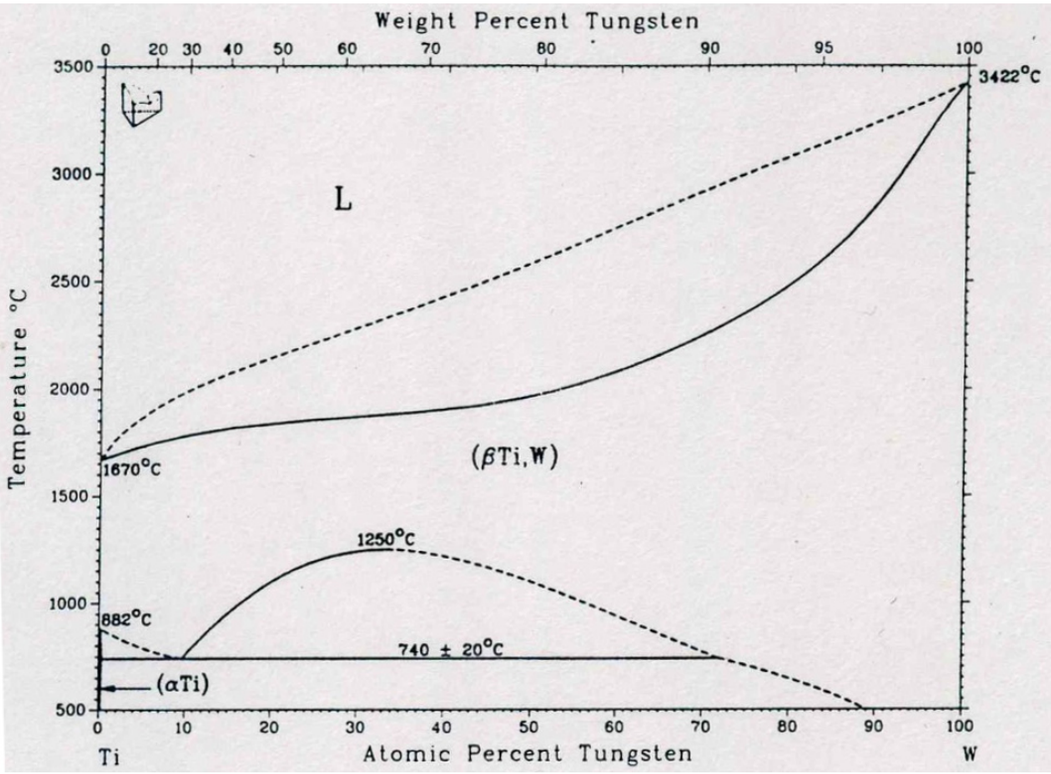

Figure 10. Equilibrium phase diagram for W and Ti. [48]

[43] In Reference 43, nanosized AlN was synthesized with an 0_2 content <0.8 wt%, while traditional methods offer AIN with an 0_2 content >5 wt%.

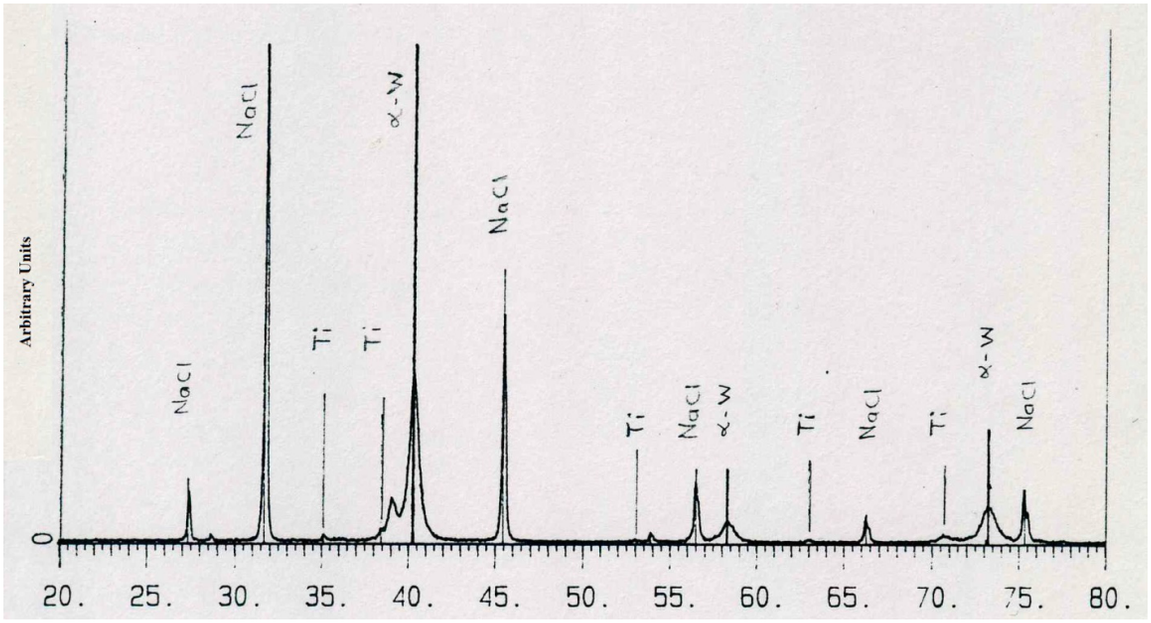

Figure 11. XRD of W-Ti sample for run No. 8.

Sample ID	Sal removal method	Residual by wt%	
		Na	Cl
W-Ti for run No 7	HT at 850°C for 10 h	0.025	0.02
W-Ti for run No 8	Water-washed	0.82	0.18

Table 3. Residual Na and Cl after salt removal of W-Ti samples as determined by elemental analysis.

In run number 8, the flow conditions were set to yield a composition of 78 wt% W and 22 wt % Ti. In this case, the XRD spectra of the as-produced sample reveals the presence of W, NaCl, and small peaks indexing to α-Ti and β-Ti (Figure 11).

6. Consolidation of W and W-Ti nanoparticles

As-produced powders were either water-washed or vacuum-annealed at 850°C, 10^{-6} torr for 2 h to sublime the protective NaCl encapsulation. The heat treatment setup used for vacuum-annealing the powders was transferred into an argon glove box for hot pressing. This procedure eliminated exposure of annealed powders to air. The nanosized W and W-Ti powders were consolidated into pellets of 6 mm diameter and 6–8 mm long.

The powders were pressed in a hot press located within the argon glove box. The hot press (Figure 12) consists of a furnace with molybdenum heating elements capable of reaching a maximum temperature of 1600°C. The hydraulic press is equipped to generate a maximum load of 225 KN.

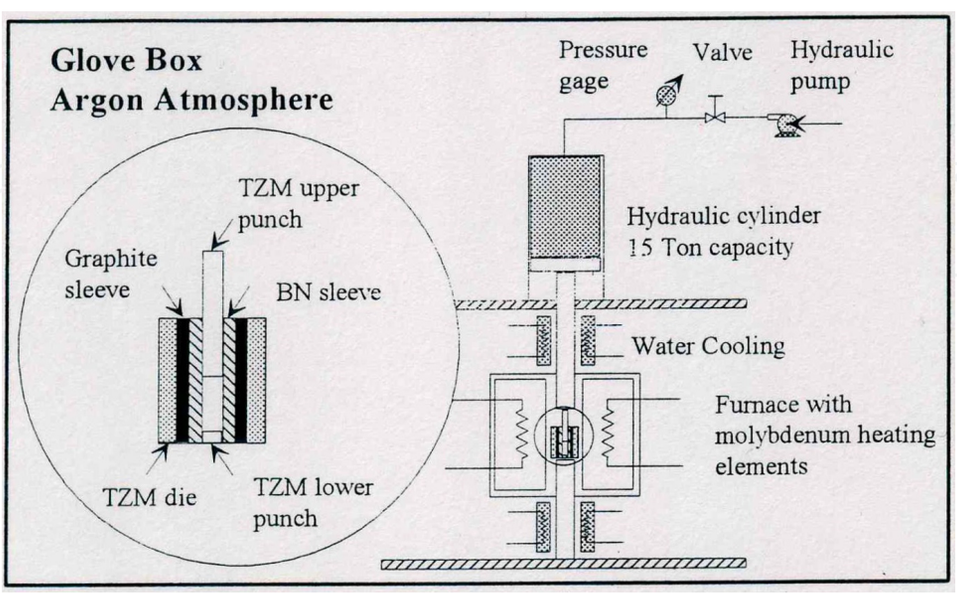

Figure 12. Hot press for consolidation of W and W-Ti particles.

http://dx.doi.org/10.5772/62023

The dies and punches used in hot pressing were made of TZM alloy (a molybdenum alloy), which has excellent high-temperature strength and oxidation resistance. A composite sleeve consisting of boron nitride (BN) and graphite was fitted into the TZM die. The inner BN sleeve minimized contamination of the W and W-Ti powders with carbon, while the outer graphite sleeve facilitated easy removal of the sample after consolidation.

The nanosized W-Ti powders were cold pressed by applying pressures up to 70 MPa. The hot pressing of the powders was carried out at 1000°C and 1200°C at a pressure of 175 MPa for 2–3 h. Table 4 summarizes the hot pressing conditions for consolidation of the W-Ti powders. After hot pressing, the consolidates were cooled slowly to room temperature and the pellets were removed from the TZM die and punch assembly. W-Ti consolidates were characterized using XRD, SEM, and TEM. The extent of densification indices were obtained by comparing the density of the consolidates to theoretical density values. Densities were measured by Archimedes principle and by measuring the dimensions of the cylindrical consolidates.

Sample	Hot Pressing Conditions			Results	
	T	P	Time	Densification	VHN
	°C	MPa	H	%	
W-13 wt% Ti No 1	1200	172	2	96	850
W-13 wt% Ti No 2	1200	172	3.5	97	800
Conventional W	N/A	N/A	N/A	100	295

Table 4. Hot pressing conditions for consolidation of the W and W-Ti powders.

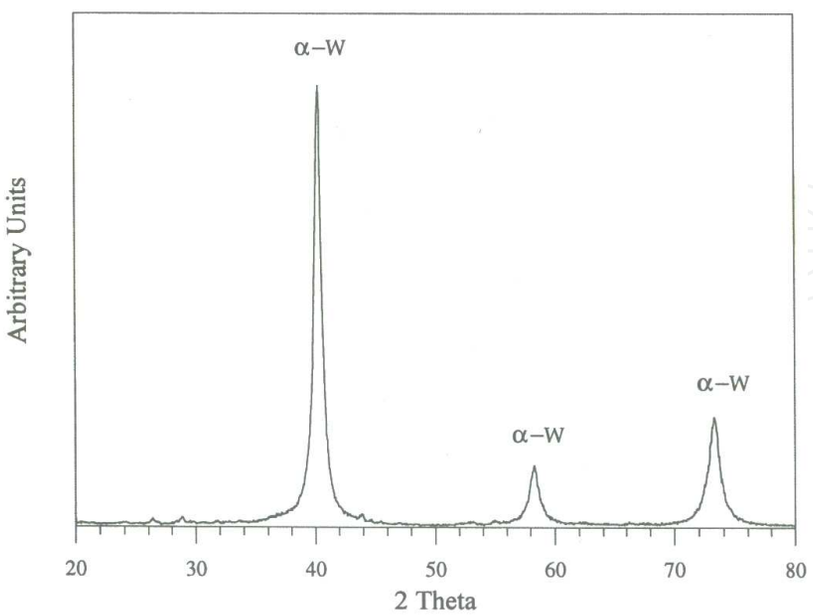

Figure 13. XRD of W-13 wt% Ti consolidated No. 2.

Figure 13 shows the XRD spectra of the W-Ti consolidate obtained under conditions No. 2. It shows broad peaks indexing to W. Figure 14 shows the SEM micrograph of the same W-Ti consolidate. As seen from the figure, the grain size of the consolidate is about 40 nm. The EDAX analysis, performed in conjunction with the SEM, shows 87 wt% W and 13% Ti. Figure 15 shows an optical micrograph of the consolidate No. 2, etched by Kcroll's reagent to show the Ti grains in the matrix. This figure shows the uniformity in the structure of the consolidate.

Though the temperatures maintained for hot pressing were between $0.36T_m$ and $0.40T_m$, the densification achieved after hot pressing was very high (~97%). Conventional materials can be consolidated to high density only by hot pressing at temperatures above ~$0.5T_m$. This shows that for WHA alloys, which possess very high melting temperatures, consolidation of nano-sized powders at relatively low temperatures into high density compacts is a viable and attractive route. Table 4 shows hardness values for nanocrystalline W and W-Ti consolidates as compared with conventional W. The hardness values are very high, as high as 4 times that of conventional W.

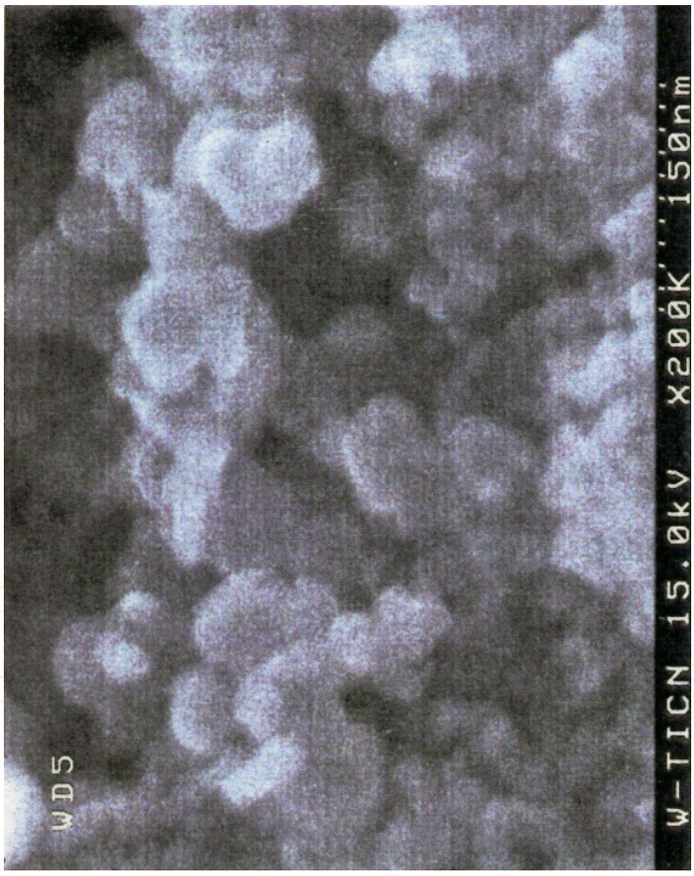

Figure 14. SEM micrograph of the W-13 wt% Ti consolidate No. 2.

The consolidated samples were hot isostatic pressed (hipped) to obtain 100% densification. Work is underway to test the mechanical properties of the fully dense consolidates under high strain rate conditions.

http://dx.doi.org/10.5772/62023

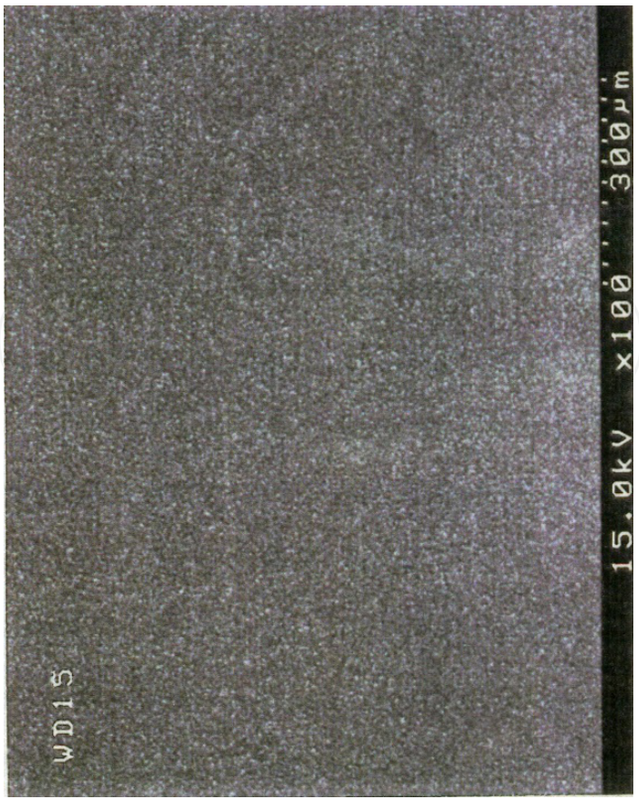

Figure 15. Optical micrograph of the W-13 wt%Ti consolidate No. 2. Etched by Kcroll's reagent to show the Ti grains in the matrix.

7. Summary

High-quality nanosized W and W-Ti nanoparticles have been produced, characterized, and consolidated to demonstrate the applicability of the sodium/halide flame synthesis and particle encapsulation process.

Nanocrystalline W particles were produced by reacting Na and WCl_6 and were characterized by XRD, SEM, TEM, and EDAX. The W particles appear unagglomerated, cubic and hexagonal in shape, and have an average size of ca. 30 nm. XRD results indicate the presence of only α-W, β-W, and NaCl. No contamination was detected even after extended exposure to atmospheric conditions. Vacuum heat treatment of the powders at 800°C results in effective removal of NaCl with no detectable change in particle size.

A powder consisting of nanosized W-Ti was also produced via $Na/WCl_6/TiC_4$ chemistry. XRD spectra of as-produced powders show only W and NaCl. EDAX indicates the presence of Ti, and analysis of lattice parameters suggests that part, not all, of the Ti is in solid solution. Particles are unagglomerated, cubic in shape, with an average size of ca. 30 nm. Heat treating the sample at 850°C increases average particle size to ca. 40 nm. When the amount of Ti is increased to 22 wt%, XRD spectra of as-produced powders show small peaks of α-Ti and β-Ti, in addition to W and NaCl. The nanosized W and W-Ti powders were successfully

consolidated into pellets of 6-mm diameter and 6–8-mm long. Densities as high as 97% were achieved by hot pressing at temperatures of $0.42T_m$ to $0.48T_m$. Microstructures of the consolidates consist of nanometer-sized grains (40 nm). Hardness measurements indicate hardness values 4 times that of conventional tungsten. A 100% densification was achieved by hipping the samples. Work is underway to test the mechanical properties of the fully dense consolidates under high strain rate conditions.

The improvement in mechanical properties of the materials produced by flame synthesis, and the experimental results showing the effectiveness of the encapsulation method to control agglomeration and purity warrant further investigation. Consequently, the following chapters are devoted to studying particle formation and encapsulation processes in two-component aerosols. A mathematical model that describes the dynamics of the aerosol will be developed and the solution of that model will provide a description of the evolution of the particles, the dominant variables controlling the processes, and the desired methodology to optimize the encapsulation process.

Author details

Jose Ignacio Huertas

Address all correspondence to: jhuertas@itesm.mx

Tecnológico de Monterrey, Mexico